Title
THz time-domain characterization of amplifying quantum-cascade metasurface

Journal
Applied Physics Letters, 119(18)

ISSN
0003-6951

Authors
Shen, Yue
Kim, Anthony D
Shahili, Mohammad
et al.

Publication Date
2021-11-01

DOI
10.1063/5.0067690

Peer reviewed

THz time-domain characterization of amplifying quantum-cascade metasurface

Yue Shen,[1, a)] Anthony D. Kim,[1] Mohammad Shahili,[1] Christopher A. Curwen,[1, 2] Sadhvikas Addamane,[3] John L. Reno,[3] and Benjamin S. Williams[1]

[1)]*Department of Electrical and Computer Engineering, University of California Los Angeles (UCLA), Los Angeles, CA 90095, USA*

[2)]*Jet Propulsion Laboratory, California Institute of Technology, Pasadena, CA 91109, USA*

[3)]*Center for Integrated Nanotechnologies, Sandia National Laboratories, Albuquerque, NM 87185, USA*

(Dated: 18 October 2021)

An amplifying quantum-cascade (QC) metasurface, the key component of the QC vertical-external-cavity surface-emitting-laser (VECSEL), is studied as a function of injected current density using reflection-mode terahertz time domain spectroscopy. Nearly perfect absorption is measured at zero bias, which is associated with the transition from the weak to strong coupling condition between the metasurface resonance and an intersubband transition within the QC material. An increase in reflectance is observed as the device is biased, both due to reduction of intersubband loss and the presence of intersubband gain. Significant phase modulation associated with the metasurface resonance is observed via electrical control, which may be useful for electrical tuning of QC-VECSEL. These results provide insight into the interaction between the intersubband QC-gain material and the metasurface, and modify the design rules for QC-VECSELs for both biased and unbiased regions.

Since the demonstration of the first terahertz (THz) QC-laser in 2002,[1] it has become a significant coherent source for imaging, sensing and spectroscopy. Devices have been demonstrated to operate so far from 1.2–5.6 THz, in a myriad of active-region and cavity configurations.[1–4] Throughout the development process, coherent THz time-domain spectroscopy (TDS) has proven to be a key characterization technique; due to the coherent nature of the electro-optic electric field sampling, direct extraction of both the amplitude and phase response is accessible.[5] For example, it has led to direct measurement of the the gain and loss characteristics of the intersubband (ISB) active medium above and below threshold, probing of gain recovery dynamics, extraction of the group velocity dispersion of the coupled active medium/waveguide system, and assisted phase-locking and injection seeding of THz QC-lasers.[6–12] Up to now, these experiments have all been performed on waveguide-based THz QC-lasers, despite the fact that it is challenging to couple the THz signal into and out of the subwavelength sized waveguides.

An external cavity configuration for THz QC-lasers has recently been developed that supports high-power operation with excellent beam quality and broadband tunability: the QC vertical-external-cavity surface-emitting-laser (VECSEL).[13–15] The key component of the QC-VECSEL is an amplifying reflectarray metasurface, which is based on a sub-wavelength array of surface radiating metal-metal waveguide antennas loaded with QC-laser gain material. In general, to maximize reflective gain, one wishes to design the metasurface resonance to spectrally align with the intersubband gain provided by the constituent active material. However, up to now the spectral properties of the QC-metasurface have been designed by simulation, and have only been verified indirectly through observation of the QC-VECSEL lasing characteristics, or by passive FTIR reflectance measurements at room-temperature.[16] Furthermore, often the simulations in question use simplified models for the material loss and the QC-gain, where uncertain Drude model parameters for material losses are used, and the detailed interaction of the intersubband transition with the metasurface is neglected.

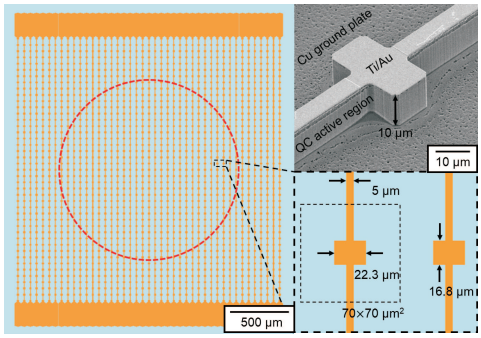

FIG. 1: Top-down schematic of the patch QC-metasurface. Only the patches (and not the connecting lines) within the red dashed circle receive electrical bias. A SEM image of a single patch and its dimensions are shown in the inset.

In this Letter, we report the use of reflection-mode THz TDS to investigate amplifying QC metasurfaces under both passive conditions and under current injection. We select for study a metasurface which has been designed for operation at 2.3 THz. While this operating frequency is lower than previously reported QC-VECSELs, it is more easily probed by THz TDS with sufficient signal-to-noise ratio (See Supplementary

a)Electronic mail: yueshen2016@ucla.edu.

Material S3). Several expected features emerge, including the existence of a metasurface resonance at the design frequency, and the compensation of the metasurface loss by intersubband gain. However, several unexpected features are also observed. Specifically, for an unbiased passive metasurface, the resonant absorption is nearly perfect — significantly stronger than expected from a simple Drude model. Additionally the unbiased condition is characterized by a dispersive reflection phase characteristic that indicates the onset of a polaritonic coupling condition between the resonant mode of metasurface and an ISB transition. These measurements have important consequences for low-loss QC-VECSEL design. They also indicate the possibility of engineering the metasurface to deliberately enhance ISB-based phase modulation or to monolithically integrate ISB based nonlinearities.

The metasurface was fabricated using the standard metal-metal waveguide process based on Cu-Cu thermocompression wafer bonding and substrate removal, as described in Refs. 13 and 17. The metasurface area is 3×3 mm^2, however only the central circular bias area of diameter 1.9 mm receives current injection and experiences gain (Fig. 1). In the remainder of the metasurface there is a layer of silicon dioxide that electrically insulates the top metal contact from the underlying semiconductor; this area remains lossy. For the purposes of this experiment, we have made the bias area as large as possible to ease alignment of the TDS beam, while keeping the total current injection to approximately 2 A (as limited by our pulse generator). To this end, instead of the traditional ridge-antenna design for the QC metasurface,[13] we adopt the patch-antenna design which is characterized by a lower overall areal fill factor, and a consequently lower power dissipation density.[18] The dimensions and an SEM image of a patch element are shown in Fig. 1. The bare metasurface without gain material is designed via finite element electromagnetic simulation to be resonant at 2.28 THz; it has a quality factor of $Q \approx 16$ which is dominated by radiative coupling. The QC-active region is based upon the hybrid bound-to-continuum/resonant-phonon design scheme designed to operate near 2.3 THz; it is grown by molecular beam epitaxy to be 10 μm thick based upon GaAs/$Al_{0.15}Ga_{0.85}$As heterostructures (wafer VA1033). The layer thicknesses in Å are **51**/109/**20**/103/**37**/88/**40**/172 (barrier layers are bold). The central 88 Å of the widest well is nominally Si doped at 5×10^{16} cm^{-3}, and capacitance-voltage measurements give an average doping of 7.6×10^{15} cm^{-3} ($\sim$7% high). Measurements on a ridge waveguide QC-laser device fabricated alongside the metasurface shows lasing in the range from 2.3–2.95 THz (see Supplementary material S4 for simulated gain spectra and S5 for *I-V* and spectral data).

As the first step, we characterize the metasurface as a full VECSEL by adding a highly-reflective output coupler ($R \sim$ 99%) to create a plano-plano Fabry-Pérot cavity with an approximate length of 1 mm. The purpose is to definitively identify the bias range over which the metasurface produces net gain, as well as identify the range of frequencies over which lasing is favored. Fig. 2 shows the voltage vs. current (*V-I*) and output light power vs. current (*L-I*) characteristics of the VECSEL characterized in pulsed mode at 77 K. The threshold current density is $J_{th} = 980$ A/cm^2 and lasing persists up

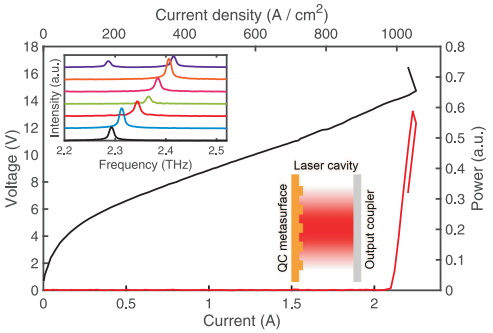

FIG. 2: (a) The *V-I* and *L-I* curves of the VECSEL at 77 K. The inset shows the lasing spectra of the VECSEL as the cavity length is tuned.

to $J_{max} = 1055$ A/cm^2, at which point a negative dynamic resistance (NDR) occurs and lasing ceases. By changing the cavity length of the VECSEL with a piezoelectric stepper, the lasing mode is tuned from 2.29 to 2.42 THz, at which point a mode-hop occurs.

Next, the output coupler is removed, and the QC metasurface is studied by reflection-mode THz TDS. The setup uses a Ti:Sapphire laser with $\sim$100 fs pulse width, 82 MHz repetition rate and 0.6 W average power to generate broadband THz pulses by pumping a large area photoconductive antenna (Tera-SED from Laser Quantum).[19] The THz probe pulse is reflected at normal incidence from the metasurface mounted in a cryostat, and reflected signal is detected using free space electro-optic sampling (1 mm thick $\langle 110 \rangle$ ZnTe crystal). A detailed schematic of the experimental setup is in the Supplementary Material S1.

Before applying a bias to the metasurface, its passive reflection spectrum was measured at 77 K. The reflected time domain field is first measured from the metasurface; then the sample cryostat is laterally translated to measure a reference spectrum from a large area uniform gold pad adjacent to the metasurface on the fabricated chip. The reflectance spectrum as well as the reflection phase are plotted as solid blue curves in Fig. 3. The most notable feature is this: the absorption dip at 2.28 THz ($R < 0.01$) is much deeper than expected, and cannot be explained by using a bulk Drude model to account for the free-carrier loss within the GaAs/AlGaAs QC-active region ($R \sim 0.3$ given 0.5 ps Drude relaxation time for GaAs and 39 fs for Au). A clue to the source of this absorption is found in examination of the dispersive zero-bias phase response shown in Fig. 3(b) (blue curve), which is characteristic of the transition from weak to the strong light-matter coupling regime.[20] In this case the coupling is between the $2 \rightarrow 3$ ISB transition and the metasurface electromagnetic resonance. The subbands in question are shown in a band diagram for one module of the active region calculated using a self-consistent Schrödinger-Poisson solver in Fig. 4(a). This particular intersubband transition exhibits a large oscillator

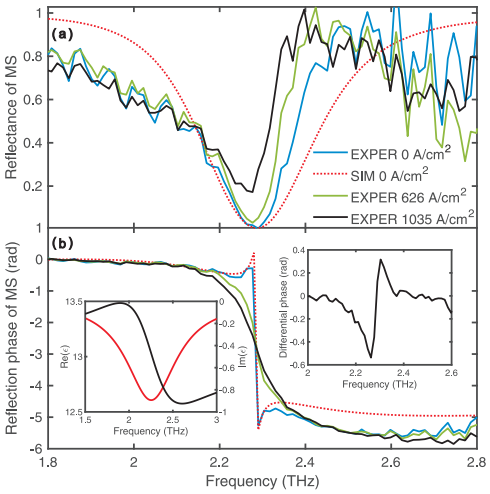

FIG. 3: (a) Reflectance and (b) reflection phase measured by THz TDS of the metasurface biased at several current density bias points (solid lines). The dotted line is a simulation result of an unbiased metasurface coupled with an ISB transition. The left inset shows the real and imaginary part of the permittivity of the active region used in finite element method simulations. The right inset shows the differential phase ($\Delta\phi_{MS}$) as the bias is switched between 626 and 1035 A/cm^2 on the metasurface.

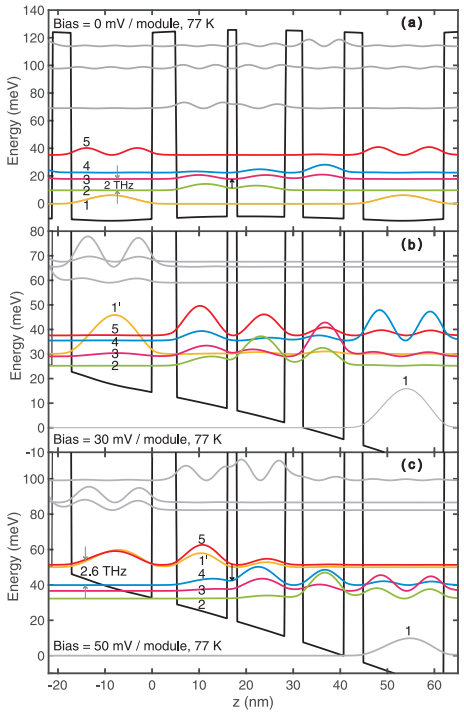

FIG. 4: Conduction band diagram of the active region at (a) zero bias and (b) subthreshold bias which approximately corresponds to the 626 A/cm^2 bias point (c) design bias at 50 mV/module which approximately corresponds to 1035 A/cm^2 bias point.

strength $f_{23} = 0.62$ at zero bias, and has an energy close to the metasurface resonance ($E_{32} \approx 9$ meV). While most of the electron population resides in subband 1, subband 2 is low enough in energy to acquire significant thermal population at 77 K.

We are able to obtain a good qualitative fitting by considering only the $2 \rightarrow 3$ ISB transition using a Lorentz oscillator model for the permittivity along the growth direction:

$$\varepsilon_z(\omega) = \varepsilon_{core} + \frac{(N_2 - N_3)e^2 f_{23}}{m^* L_{mod}} \frac{1}{\omega_{23}^2 - \omega^2 - i\omega\gamma}, \quad (1)$$

where ε_{core} is the semiconductor permittivity excluding free carrier contributions, N_3 and N_2 are the 2D subband populations (thermally populated at zero bias), m^* is the GaAs electron effective mass, L_{mod} is the width of the module of active region, $\hbar\omega_{23}$ is the intersubband transition energy and γ is the damping term. This is shown in the left inset of Fig. 3(b) for the chosen parameters $N_2 - N_3/L_{mod} = 1.9 \times 10^{15}$ cm^{-3}, $\gamma = 2\pi \times 700$ GHz. To obtain the best fit with the data, we adjusted the ISB frequency $\omega_{23} = 2.28$ THz to match the metasurface resonance. While this is 0.2 THz higher than the result from Schrödinger simulations, the adjustment is reasonable given uncertainties in growth thicknesses and compositions of the QC-material. This permittivity is used to simulate the reflectance and reflection phase of the passive MS using finite element method via Ansys HFSS. The simulation results displayed in Fig. 3 (red dotted curve) show a good fit with the phase characteristics, and reproduce the nearly perfect absorption at 2.3 THz. We describe this as the transition between weak and strong coupling regime; considering the metasurface linewidth, the carrier density is too low to observe an unambiguous Rabi splitting in absorption spectrum.[21] See Supplementary material S6 for further simulations of predicted reflection characteristics as a function of ISB population.

Next, we consider the optical response of the metasurface under electrical bias. The reflectance and reflection phase are plotted at two additional bias points in Fig. 3. At $J = 626$ A/cm^2, the active region is biased in the sub-threshold "leakage" alignment, which roughly corresponds to the band condition shown in Fig. 4(b) where current is injected into the lower radiative states subbands 3 and 4. While the reflectance spectrum continues to show strong absorption, the reflection phase changes considerably and returns to a more conventional Lorentzian phase response. This indicates that the metasurface has entered the weak-coupling regime, as the $2 \rightarrow 3$

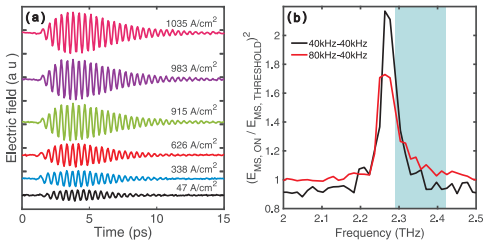

FIG. 5: (a) The differential electric fields in the time-domain ($E_{MS,on}$ - $E_{MS,off}$) of the metasurface measured using lock-in detection for different current densities. (b) The relative gain of the metasurface biased above threshold ($J = 1035$ A/cm^2) relative to the reflectance biased near threshold ($J = 983$ A/cm^2) using data extracted from two biasing schemes described in Supplemental material S2. The blue shaded region indicates the VECSEL lasing frequency range from 2.29 to 2.42 THz where we can be confident that the metasurface reflectance is near unity at threshold.

ISB transition redshifts away from the metasurface resonance at 2.28 THz, and the population of level 2 decreases. At $J = 1035$ A/cm^2, the active region is biased into the "design" alignment which is shown in Fig. 4(c). Here, current is injected into the upper radiative subband 5, and gain occurs on the $5 \rightarrow 4$ and $5 \rightarrow 3$ transitions. And indeed, the measured reflectance spectrum in Fig. 3(a) shows an increase in the reflectance, particularly on the high-frequency side of the resonance feature where it approaches unity in the 2.35–2.45 THz range. However, contrary to expectations, the absorption feature is never fully compensated by gain. This asymmetric change in reflectance is likely due to the fact that the ISB gain transitions are centered mostly at higher frequencies (as is confirmed by the measurement of the ridge waveguide lasing frequencies from 2.3–2.95 THz in the Supplementary material S5). This is consistent with the fact that the VECSEL lasing was found to occur only between 2.29–2.42 THz — a range above the metasurface central resonant frequency.

However, a natural question arises: why is an unambiguous reflectance $R > 1$ not measured when we know lasing occurs in a VECSEL? There are several explanations. First, since the measurement of the metasurface VECSEL used an output coupler with ∼99% reflectance, this requires that the metasurface have only $R \geq 1.01$ between 2.29 and 2.42 THz for lasing to occur. This is a small signal which may be obscured by the reduced TDS SNR that occurs at high frequencies. Second, only the central circular area (diameter 1.9 mm) receives electrical bias. Analysis of the TDS time-domain signal indicates even at our best alignment, the illumination spot is not ideal and some portion of the incident THz beam spills over onto the unbiased area of the metasurface where it is strongly absorbed (Supplementary material S3). As a result, the overall measured reflectance is underestimated.

Finally, in order to isolate the effect of the metasurface bias, we performed differential TDS spectroscopy in a synchronous pulse scheme, where the metasurface bias is modulated at half the frequency of the photoconductive antenna, so that lock-in detection can be used to measure the differential electric fields $E_{MS,on}$ - $E_{MS,off}$ (shown in Fig. 5(a)). A detailed description of the biasing scheme is in the Supplementary material S2, and is similar to that in Ref. 22. Generally speaking, the oscillations lasts longer and the amplitude of oscillations increases as the bias increases. At low biases, this is a result of the loss reduction, and at higher biases, the result of QC gain. Unlike in previous measurements of waveguide QC-lasers, by itself this type of differential measurement is not effective at isolating the absolute QC-gain since the off-state of the metasurface is characterized by the strong resonant absorption.[22] Instead, in Fig. 5(b) we plot the relative gain of the metasurface obtained by taking the ratio of the reflectance at the maximum bias $J = 1035$ A/cm^2 to that at bias $J = 983$ A/cm^2 which is very close to the VECSEL threshold current density (see Fig. 2). Near the threshold bias, we can be sure that the reflectance within the bias area is very close to unity (at least in the range where lasing occurs from 2.29–2.42 THz), and hence is suitable to use as a reference. We perform this calculation using both biasing schemes described in Supplemental material S2: differential biasing and absolute biasing. We have fairly high confidence in the values of the gain within the range 2.29–2.42 THz (blue shaded region in Fig. 5(b)); outside this region we cannot be sure that the metasurface reflectance at 983 A/cm^2 is close to unity and thus the given value almost certainly overestimates the absolute gain.

These results are highly informative for future QC-VECSEL design. First, it is now clear that the absorbance of the unbiased portions of the metasurface is much higher than previously understood.[16] Considering only the metallic loss, or using a Drude model to approximate free-carrier loss within the semiconductor is insufficient and cannot capture polaritonic and strong-coupling phenomena. One must consider the ISB transitions within the unbiased active region specifically, which in turn means a particular metasurface must be tailored to a particular QC active region design. This is uniquely important for a QC-VECSEL, in which the wings of the cavity mode are expected to interact with the unbiased metasurface; this will introduce extra cavity loss as well as cause the cavity mode to "gain-guide" and try to confine itself to the biased area.[23] This is a phenomenon which is not typically observed with a ridge waveguide THz QC-laser. Future metasurface designs can potentially accommodate this both by optimizing the metasurface antenna design in the unbiased area to reduce this loss, as well as by redesigning active regions to ensure that lossy ISB transitions don't couple with the metasurface. Second, the coupling of the ISB transition with the metasurface results in a large electrically controlled amplitude and phase modulation. For example, if we consider the metasurface as an amplitude modulator, the nearly perfect absorption results in a modulation index of close to unity. Phase modulation is significant also. For example, at 2.26 THz (just below resonance frequency), from zero bias to 626 A/cm^2, 1.1 radians of tuning is observed as the the strong coupling condition is removed, and from 626 A/cm^2 to 1035 A/cm^2, 0.5 radians of tuning is observed related to the build-up of the population in-

verted ISB transition for lasing (see Fig. 3(b) inset). The latter phase shift co-exists with ISB gain and suggests that proper engineering of the metasurface and ISB transition could be used for fast electrical tuning or frequency stabilization of the QC-VECSEL.[24,25] Finally, there has been a great deal of recent attention of the nonlinear optical properties of ISB polaritonic metasurfaces (e.g. for frequency mixing, saturable absorption, optical limiting).[26–28] Our results suggest the possibility of integrating saturable absorption or effective Kerr nonlinearities within the QC-VECSEL laser cavity through modal interactions with the unbiased portions of the metasurface.

SUPPLEMENTARY

See supplementary material for details on the THz TDS experimental setup and data processing, numerical modeling of the QC active region gain and refractive index, experimental laser spectra for metal-metal ridge waveguide device from the same active material, and electromagnetic modeling of a coupled ISB/metasurface system.

DATA AVAILABILITY

The data that supports the findings of this study are available within the article (and its supplementary material).

ACKNOWLEDGMENTS

The authors would like to thank Nezih Tolga Yardimci and Mona Jarrahi for assistance with THz TDS setup, Luyao Xu for assistance with experimental setup and Yu Wu for ridge waveguide testing. Microfabrication was performed at the UCLA Nanoelectronics Research Facility and wire bonding was performed at the UCLA Center for High Frequency Electronics. This work was performed, in part, at the Center for Integrated Nanotechnologies, an Office of Science User Facility operated for the U.S. Department of Energy (DOE) Office of Science. Sandia National Laboratories is a multimission laboratory managed and operated by National Technology and Engineering Solution of Sandia, LLC., a wholly owned subsidiary of Honeywell International, Inc., for the U.S. Department of Energy's National Nuclear Security Administration under contract DE-NA-0003525. Partial funding was provided by the National Science Foundation (1711892, 1810163) and National Aeronautics and Space Administration (80NSSC19K0700).

CONFLICT OF INTEREST

The authors have no conflicts to disclose.

[1]R. Köhler, A. Tredicucci, F. Beltram, H. E. Beere, E. H. Linfield, A. G. Davies, D. A. Ritchie, R. C. Iotti, and F. Rossi, "Terahertz semiconductor-heterostructure laser," Nature **417**, 156–159 (2002).
[2]J. Faist, M. Beck, T. Aellen, and E. Gini, "Quantum-cascade lasers based on a bound-to-continuum transition," Applied Physics Letters **78**, 147–149 (2001).
[3]B. S. Williams, H. Callebaut, S. Kumar, Q. Hu, and J. L. Reno, "3.4-thz quantum cascade laser based on longitudinal-optical-phonon scattering for depopulation," Applied Physics Letters **82**, 1015–1017 (2003).
[4]B. S. Williams, S. Kumar, H. Callebaut, Q. Hu, and J. L. Reno, "Terahertz quantum-cascade laser at $\lambda \approx 100$ μm using metal waveguide for mode confinement," Applied Physics Letters **83**, 2124–2126 (2003).
[5]J. Kröll, J. Darmo, S. S. Dhillon, X. Marcadet, M. Calligaro, C. Sirtori, and K. Unterrainer, "Phase-resolved measurements of stimulated emission in a laser," Nature **449**, 698–701 (2007).
[6]J. Kröll, J. Darmo, K. Unterrainer, S. S. Dhillon, C. Sirtori, X. Marcadet, and M. Calligaro, "Longitudinal spatial hole burning in terahertz quantum cascade lasers," Applied Physics Letters **91**, 161108 (2007).
[7]N. Jukam, S. Dhillon, D. Oustinov, Z.-Y. Zhao, S. Hameau, J. Tignon, S. Barbieri, A. Vasanelli, P. Filloux, C. Sirtori, and X. Marcadet, "Investigation of spectral gain narrowing in quantum cascade lasers using terahertz time domain spectroscopy," Applied Physics Letters **93**, 101115 (2008).
[8]N. Jukam, S. Dhillon, D. Oustinov, J. Madéo, J. Tignon, R. Colombelli, P. Dean, M. Salih, S. Khanna, E. Linfield, and A. G. Davies, "Terahertz time domain spectroscopy of phonon-depopulation based quantum cascade lasers," Applied Physics Letters **94**, 251108 (2009).
[9]D. Burghoff, T.-Y. Kao, D. Ban, A. W. M. Lee, Q. Hu, and J. Reno, "A terahertz pulse emitter monolithically integrated with a quantum cascade laser," Applied Physics Letters **98**, 061112 (2011).
[10]M. Martl, J. Darmo, C. Deutsch, M. Brandstetter, A. M. Andrews, P. Klang, G. Strasser, and K. Unterrainer, "Gain and losses in THz quantum cascade laser with metal-metal waveguide," Optics Express **19**, 733–738 (2011).
[11]D. Oustinov, N. Jukam, R. Rungsawang, J. Madéo, S. Barbieri, P. Filloux, C. Sirtori, X. Marcadet, J. Tignon, and S. Dhillon, "Phase seeding of a terahertz quantum cascade laser," Nature communications **1**, 1–6 (2010).
[12]J. Maysonnave, N. Jukam, M. S. M. Ibrahim, R. Rungsawang, K. Maussang, J. Madéo, P. Cavalié, P. Dean, S. P. Khanna, D. P. Steenson, *et al.*, "Measuring the sampling coherence of a terahertz quantum cascade laser," Optics Express **20**, 16662–16670 (2012).
[13]L. Xu, C. A. Curwen, P. W. Hon, Q.-S. Chen, T. Itoh, and B. S. Williams, "Metasurface external cavity laser," Applied Physics Letters **107**, 221105 (2015).
[14]C. Curwen, J. Reno, and B. Williams, "Broadband continuous single-mode tuning of a short-cavity quantum-cascade VECSEL," Nature Photonics **13**, 855–859 (2019).
[15]C. Curwen, J. Reno, and B. Williams, "Terahertz quantum cascade VECSEL with watt-level output power," Nature Photonics **113**, 011104 (2018).
[16]L. Xu, C. A. Curwen, D. Chen, J. L. Reno, T. Itoh, and B. S. Williams, "Terahertz metasurface quantum-cascade VECSELs: theory and performance," IEEE Journal of Selected Topics in Quantum Electronics **23**, 1–12 (2017).
[17]B. S. Williams, S. Kumar, Q. Hu, and J. L. Reno, "Operation of terahertz quantum-cascade lasers at 164 K in pulsed mode and at 117 K in continuous-wave mode," Optics Express **13**, 3331–3339 (2005).
[18]C. A. Curwen, J. L. Reno, and B. S. Williams, "Terahertz quantum-cascade patch-antenna VECSEL with low power dissipation," Applied Physics Letters **116**, 241103 (2020).
[19]A. Dreyhaupt, S. Winnerl, T. Dekorsy, and M. Helm, "High-intensity terahertz radiation from a microstructured large-area photoconductor," Applied Physics Letters **86**, 121114 (2005).
[20]J. B. Khurgin, "Exceptional points in polaritonic cavities and subthreshold Fabry–Pérot lasers," Optica **7**, 1015–1023 (2020).
[21]Y. Todorov, A. M. Andrews, I. Sagnes, R. Colombelli, P. Klang, G. Strasser, and C. Sirtori, "Strong light-matter coupling in subwavelength metal-dielectric microcavities at terahertz frequencies," Phys. Rev. Lett. **102**, 186402 (2009).
[22]N. Jukam, S. Dhillon, Z.-Y. Zhao, G. Duerr, J. Armijo, N. Sirmons, S. Hameau, S. Barbieri, P. Filloux, C. Sirtori, , X. Marcadet, and J. Tignon, "Gain measurements of THz quantum cascade lasers using THz time-domain spectroscopy," IEEE Journal of Selected Topics in Quantum Electronics **14**, 436–442 (2008).
[23]Y. Wu, Y. Shen, S. Addamane, J. L. Reno, and B. S. Williams, "Tunable quantum-cascade vecsel operating at 1.9 THz," manuscript under review (2021).

PLEASE CITE THIS ARTICLE AS DOI: 10.1063/5.0067690

[24]D. Turčinková, M. I. Amanti, G. Scalari, M. Beck, and J. Faist, "Electrically tunable terahertz quantum cascade lasers based on a two-sections interdigitated distributed feedback cavity," Applied Physics Letters **106**, 131107 (2015).

[25]L. Gao, L. Zhao, J. L. Reno, and S. Kumar, "Electrical tuning of a terahertz quantum cascade laser based on detuned intersubband absorption," Applied Physics Letters **115**, 141102 (2019).

[26]J. Raab, F. P. Mezzapesa, L. Viti, N. Dessmann, L. K. Diebel, L. Li, A. G. Davies, E. H. Linfield, C. Lange, R. Huber, and M. S. Vitiello, "Ultrafast terahertz saturable absorbers using tailored intersubband polaritons," Nature Communications **11**, 4290 (2020).

[27]S. A. Mann, N. Nookala, S. C. Johnson, M. Cotrufo, A. Mekawy, J. F. Klem, I. Brener, M. B. Raschke, A. Alù, and M. A. Belkin, "Ultrafast optical switching and power limiting in intersubband polaritonic metasurfaces," Optica **8**, 606–613 (2021).

[28]R. Sarma, N. Nookala, K. J. Reilly, S. Liu, D. de Ceglia, L. Carletti, M. D. Goldflam, S. Campione, K. Sapkota, H. Green, G. T. Wang, J. Klem, M. B. Sinclair, M. A. Belkin, and I. Brener, "Strong coupling in all-dielectric intersubband polaritonic metasurfaces," Nano Letters **21**, 367–374 (2021).

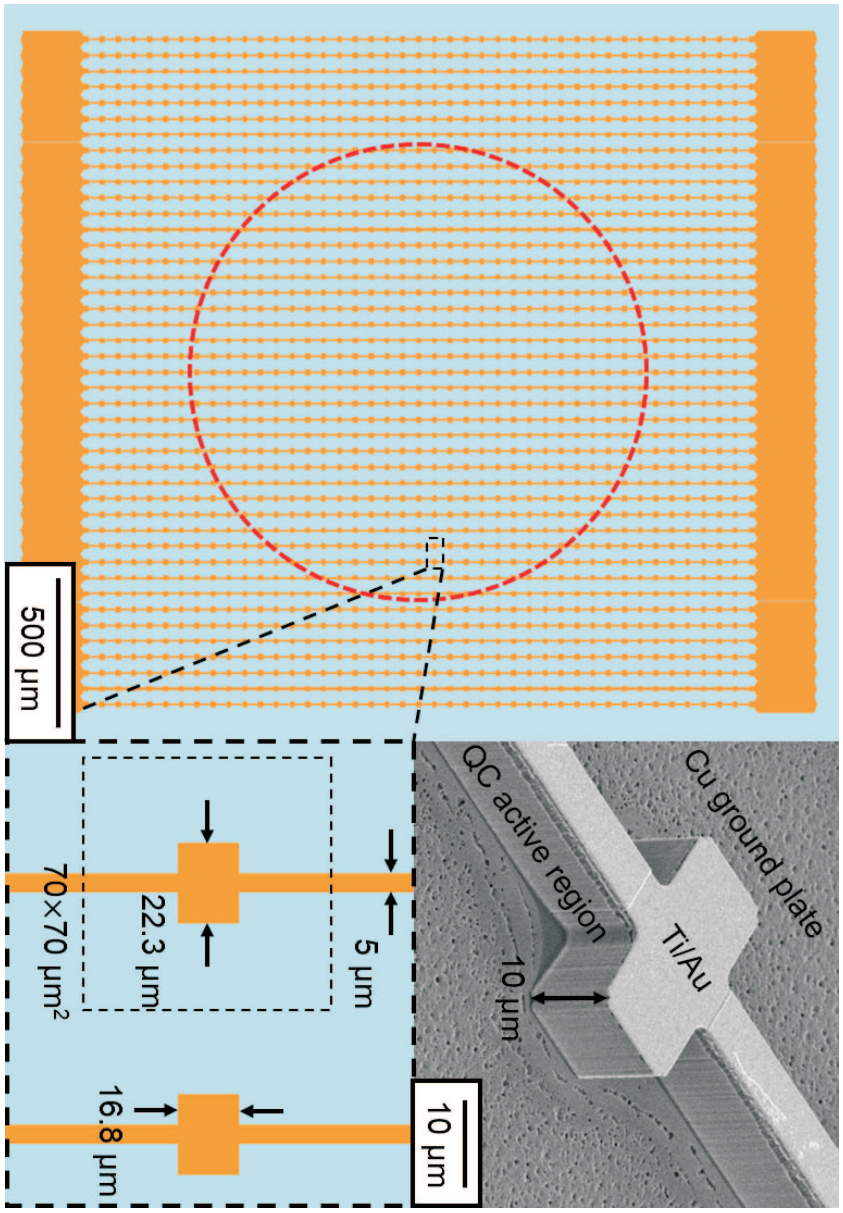

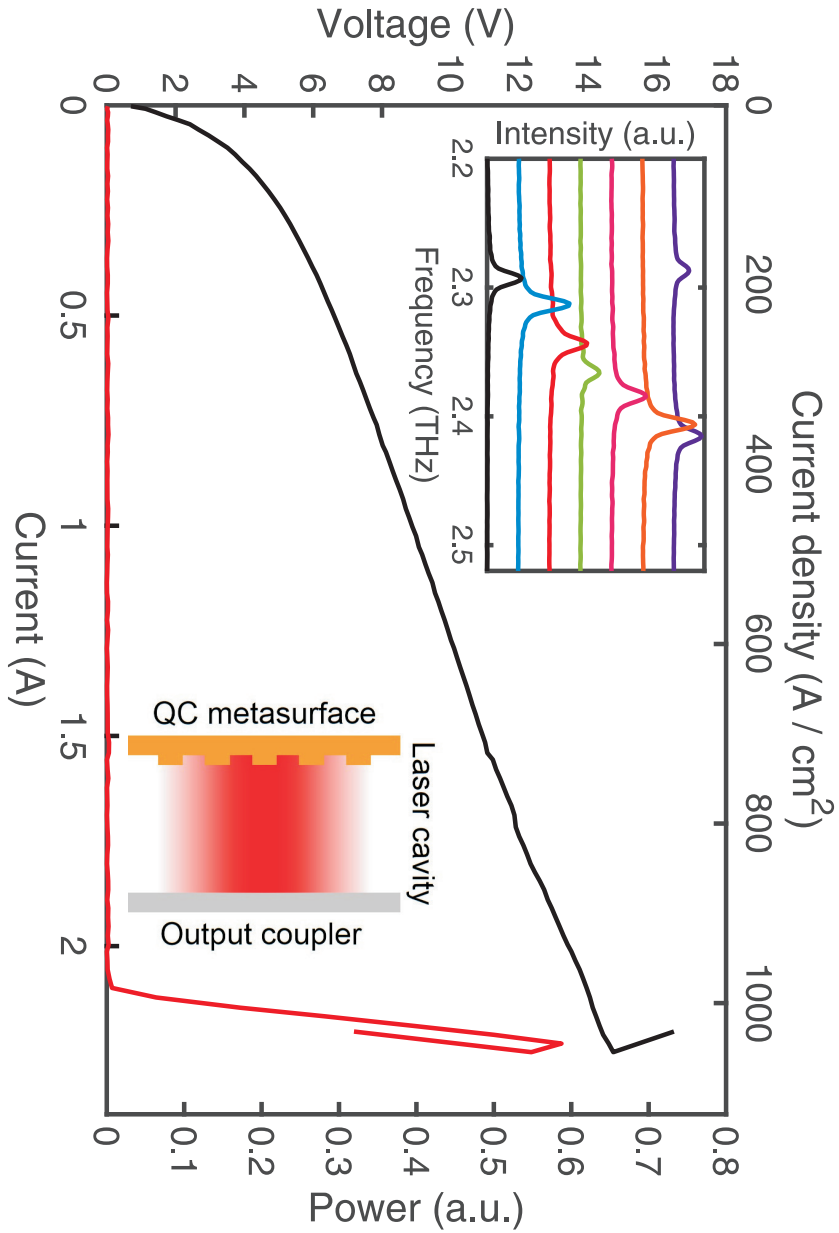

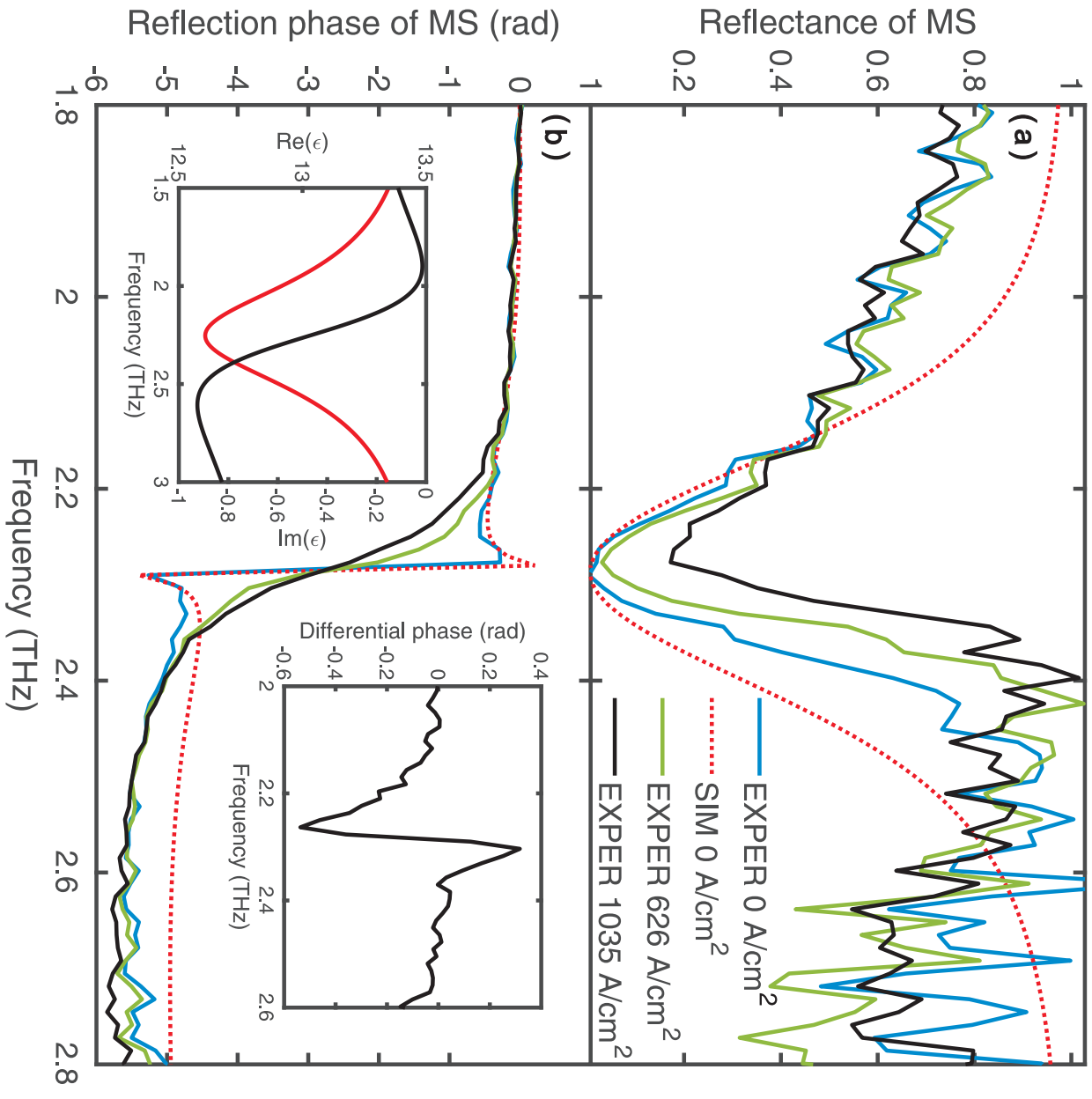

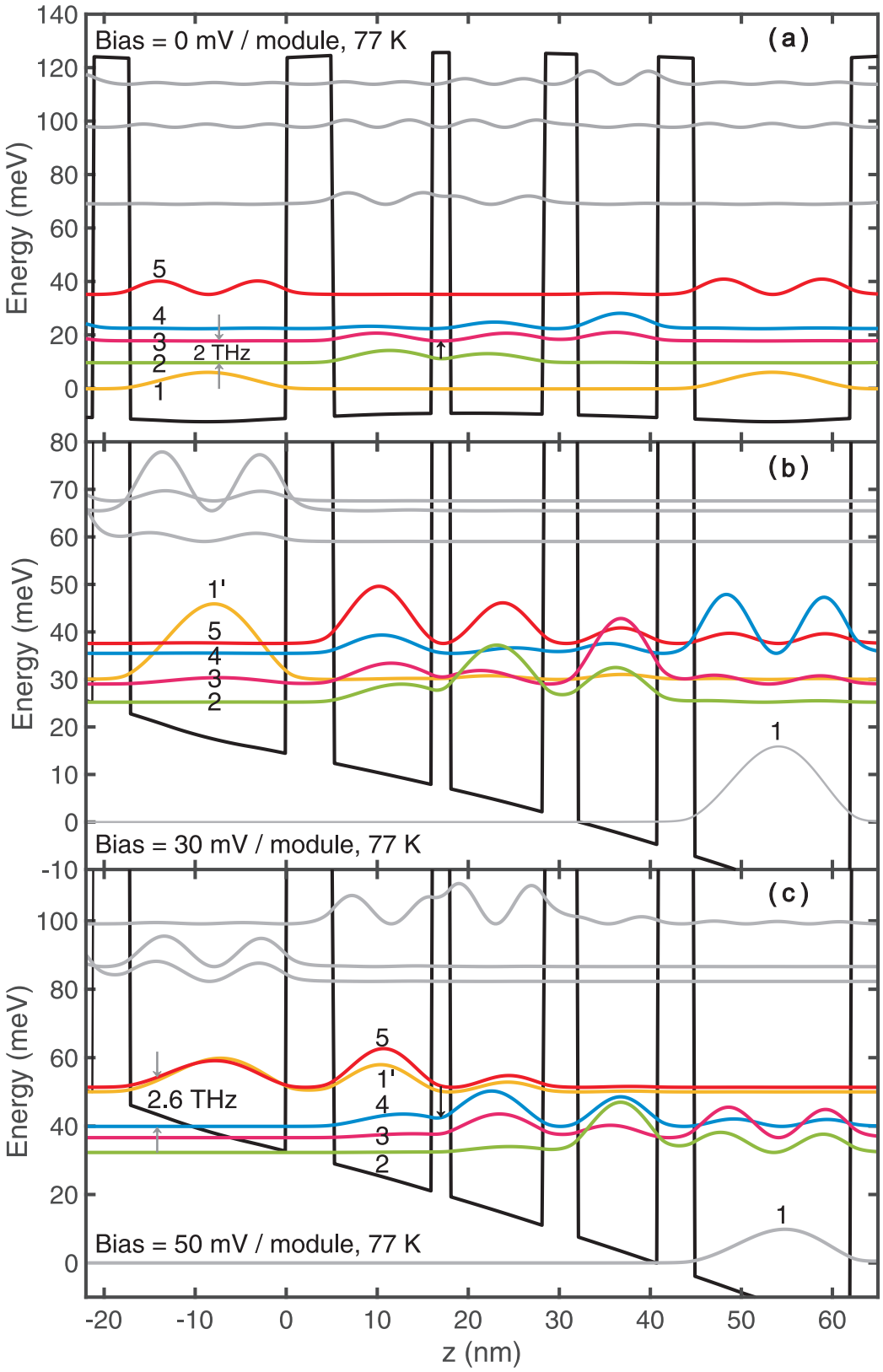

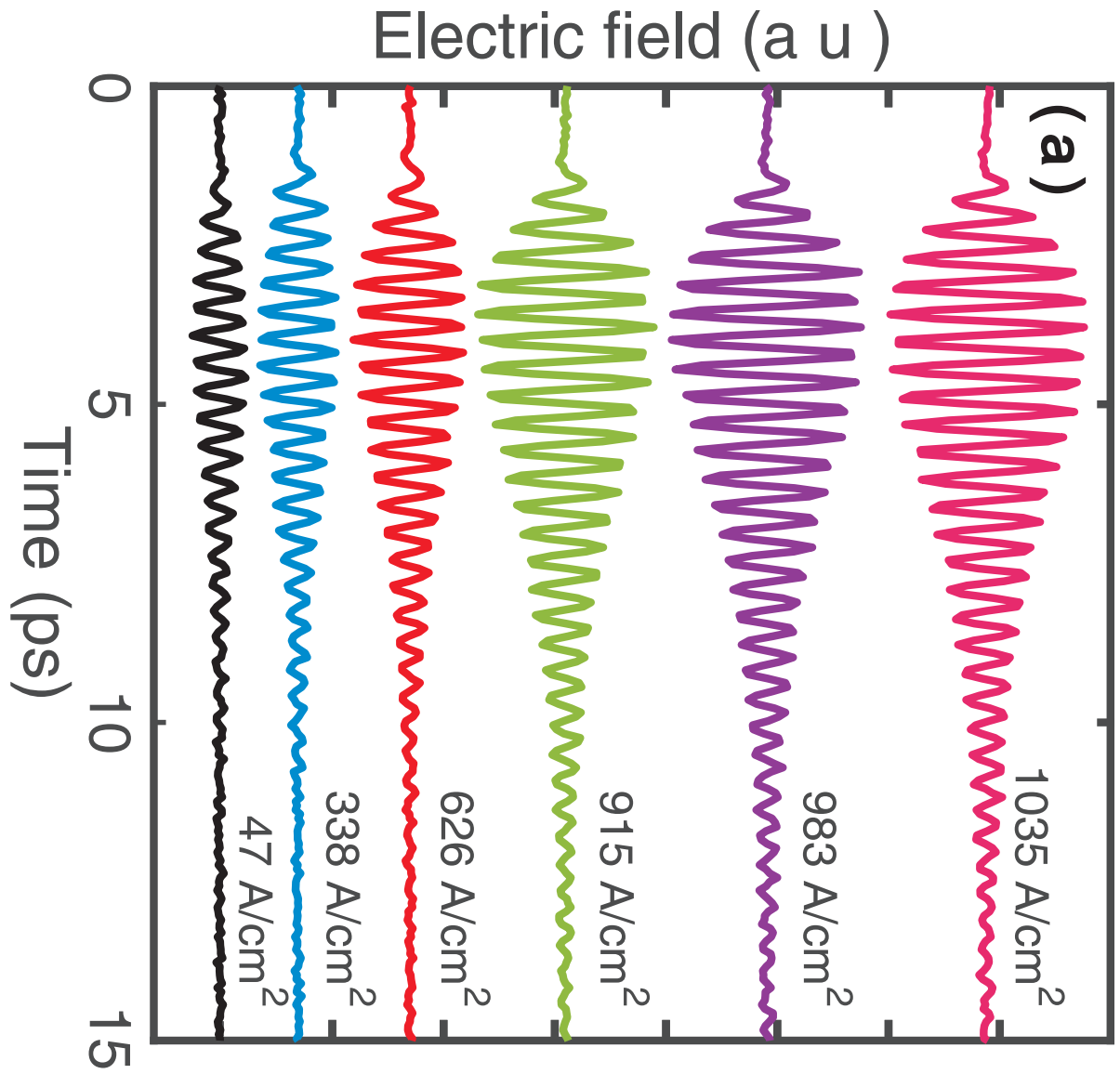

PLEASE CITE THIS ARTICLE AS DOI: 10.1063/5.0067690